A seasonal transition in biological carbon pump efficiency in the northern Scotia Sea, Southern Ocean

Stephanie A. Henson [a,*], Nathan Briggs [a], Filipa Carvalho [a], Clara Manno [b], Alexandre Mignot [c], Sandy Thomalla [d]

[a] *National Oceanography Centre, Southampton, UK*
[b] *British Antarctic Survey, Cambridge, UK*
[c] *Mercator Ocean International, Toulouse, France*
[d] *Southern Ocean Carbon and Climate Observatory, Cape Town, South Africa*

ARTICLE INFO

Handling Editor: Prof. J Aristegui

ABSTRACT

The biological carbon pump (BCP) contributes to the oceanic CO_2 sink by transferring particulate organic carbon (POC) into the deep ocean. The magnitude and efficiency of the BCP is likely to vary on timescales of days to seasons, however characterising this variability from shipboard observations is challenging. High resolution, sustained observations of primary production and particle fluxes by autonomous vehicles offer the potential to fill this knowledge gap. Here we present a 4 month, daily, 1 m vertical resolution glider dataset, collected in the high productivity bloom, downstream of South Georgia, Southern Ocean. The dataset reveals substantial temporal variability in primary production, POC flux and attenuation. During the pre-bloom peak phase we find high export efficiency, implying minimal heterotrophic POC consumption, i.e. productivity is decoupled from upper ocean remineralisation processes. As the bloom progresses from its peak through its declining phase, export flux decreases, but transfer efficiency within the upper 100 m of the mesopelagic increases. Conversely, transfer efficiency in the lower mesopelagic decreases in the post-bloom phase, implying that the flux attenuation processes operating in the upper and lower mesopelagic are effectively decoupled. This finding underscores an important limitation of using a single parameter, such as Martin's 'b', to characterise POC flux attenuation in a given location or season. Frequent pulses of export flux are observed throughout the deployment, indicating decoupling between primary production and the processes driving export of material from the upper ocean. The mechanisms underlying the observed seasonal changes in BCP magnitude and efficiency are unclear, as temperature and oxygen concentration changed minimally, although the nature of the sinking particles changed substantially as the bloom progressed. Our results highlight the difficulty of capturing temporal variability and episodic flux events with traditional shipboard observations, which affects our conceptual understanding of the BCP. The increasing use of autonomous vehicles to observe particle fluxes will be essential to characterising the temporal variability in magnitude and functioning of the BCP.

1. Introduction

The sinking of organic matter generated by primary producers out of the upper ocean and into the mesopelagic zone contributes to the oceanic sink of CO_2. Without this biological carbon pump (BCP), atmospheric CO_2 levels could be up to 50% higher than they currently are (Parekh et al., 2006). CO_2 is fixed into particulate organic carbon (POC) through primary production (PP) in the ocean's upper productive layer. A fraction of the POC sinks into the mesopelagic layer (termed export

flux), where remineralisation of the material occurs through zooplankton and microbial activity. The remaining fraction of POC flux may be transferred out of the mesopelagic layer (setting the "efficiency" of the BCP) and the associated carbon may be stored out of contact with the atmosphere for decades to millennia. Temporal variability, over days to seasons, in the magnitude and efficiency of the BCP have been posited (e.g. Smetacek et al., 1978; Heimbürger et al., 2013; Giering et al., 2017; Henson et al., 2015), following the observation that the 'input' to the biological carbon pump (primary production) varies on daily to seasonal

timescales, as do factors contributing to the magnitude of export flux and its attenuation. Improved characterisation of the daily-to-seasonal variability in the BCP should shed light on the mechanistic drivers of BCP magnitude, and elucidate the role of episodic events in food supply to the mesopelagic and benthic ecosystems.

However, temporal variability in BCP efficiency is very challenging to assess using conventional approaches (e.g. arrays of neutrally buoyant drifting sediment traps) as vertical profiles of fluxes are needed, and instruments must be deployed and recovered during research cruises which are limited to a few weeks' duration, severely limiting the quantity and temporal coverage of data. The most recent compilation of direct observations of BCP efficiency made using arrays of drifting sediment traps comprises just 24 data points, all collected in the Northern Hemisphere over 1–3 day periods (Wiedmann et al., 2020), a very small number with which to characterise variability in a key climate regulation factor. Although compilations of hundreds of ^{234}Th and drifting sediment trap profiles have generated global scale estimates of export flux and export efficiency (export flux/PP; Le Moigne et al., 2013; Mouw et al., 2016), these data similarly suffer from significant sampling bias due to ship logistical constraints, cannot provide information on (sub)seasonal variability, and furthermore do not measure deep sequestration flux. On the other hand, moored sediment traps can characterise deep (generally ≥2000 m) POC flux on hourly to inter-annual timescales (e.g. McGill et al., 2016; Hartman et al., 2021; Honda et al., 2002; Smith et al., 2018), but are geographically limited and cannot measure export flux or mesopelagic transfer efficiency.

Despite the paucity of data, the importance of POC flux attenuation in the global carbon cycle has led to efforts to extrapolate the limited available data to the global scale, generally using satellite data (e.g. Guidi et al., 2015; Henson et al., 2012a,b; Marsay et al., 2015). These efforts have resulted in opposing predicted patterns in flux attenuation, with both strong attenuation at high latitudes (and low attenuation at low latitudes; Guidi et al., 2015; Henson et al., 2012a; Mouw et al., 2016) and the exact opposite pattern being proposed (Cram et al., 2018; DeVries and Weber, 2017; Marsay et al., 2015). These contradictory predictions of how flux attenuation varies clearly highlight that our current understanding of an important planetary carbon flux is incomplete.

Inherent in many of these extrapolations is the assumption that flux attenuation is temporally invariant, i.e. the value obtained for a specific region during a particular cruise or sampling campaign is assumed to be representative of the seasonal or annual mean. However, model studies suggest that overlooking temporal variability in export efficiency (export flux/PP) may lead to substantial errors in estimates of annual mean export of up to ± 60%, with highest values occurring in regions of strong seasonality (Henson et al., 2015). Similarly, estimates of the mesopelagic net organic carbon supply are also influenced by assuming time invariance, with net POC supply potentially overestimated (underestimated) by up to 25% before (after) the bloom peak in seasonally variable systems (Giering et al., 2017).

Continuous, high frequency measurements of particle export and attenuation are clearly needed to resolve temporal variability and understand the uncertainties arising from overlooking it. Autonomous underwater vehicles have the potential to deliver this understanding, and evidence that temporal variability in flux attenuation may be substantial and regionally variable is starting to emerge from both biogeochemical Argo float and glider datasets. For example, in the northeast Atlantic, small-particle flux attenuation was found to be lowest in winter and high during the spring bloom (Bol et al., 2018), whereas in the subtropical Atlantic flux attenuation was lower during the bloom period than outside of it (Estapa et al., 2019). The GOCART project (Gauging Ocean organic Carbon Attenuation using Robotic Technologies) undertook a multi-month glider mission spanning spring and summer in a highly seasonally variable region of the Southern Ocean. The glider deployment overlapped with the COMICS cruise (Controls over Ocean Mesopelagic Interior Carbon

Storage; Sanders et al., 2016), which ensured abundant *in situ* data for calibration and validation. The target region was an area downstream of South Georgia, an island in the Atlantic sector of the Southern Ocean, in the northern Scotia Sea. This region is a hotspot of biological productivity (and associated carbon export), fuelled by an island-derived iron supply, which supports a diverse food-web (e.g. Atkinson et al., 2001; Borrione and Schlitzer, 2013). This manuscript gives an overview of the South Georgia glider deployment and an assessment of the temporal variability in primary production, export flux and its attenuation in the mesopelagic over a 4-month period spanning the spring phytoplankton bloom.

2. Methods

2.1. Glider deployments

Three gliders were deployed downstream of South Georgia, Southern Ocean near the long-term mooring site P3 (Manno et al., 2022) in conjunction with the COMICS1 cruise (DY086), which focused on sampling particle fluxes, the pelagic community and mesopelagic remineralisation processes. The region of our glider deployments was sampled from the RRS *Discovery* between 15 November and 15 December 2017 in 3 sampling periods, or epochs: P3A from 15 to 22 November 2017, P3B from 29 November to 5 December 2017, and P3C from 9 to 15 December 2017.

A Seaglider was deployed on 19 October 2017 from the South Georgia fisheries vessel, *Pharos*. Two Slocum G2s were deployed subsequently from the RRS *Discovery* on 15 November and 29 November 2017. The Seaglider was recovered from the RRS *Discovery* on 2 December 2017, with the two Slocums recovered on 13 February 2018 from RRS *James Clark Ross*. The three gliders followed a triangular path with sides of ~12 km, centred on 52.75 °S, 40.16 °W (Fig. 1), with the 2 Slocum gliders moving in opposite directions around the triangle. A complete circuit of the triangle was completed by a glider in ~3 days. Each glider was equipped with sensors for temperature, salinity, dissolved oxygen concentration, light, chlorophyll fluorescence and particulate optical backscattering at 700 nm ($b_{bp}700$). Details of the sensors and sampling frequency of each glider are in Table S1. Of note is that the Seaglider, which was initially sampling our region solo, had lower sampling frequency than the Slocum gliders, leading to lower precision (greater variability) in the flux estimates prior to 15 November.

The Supplementary Material provides details of the inter-calibration of the 3 glider datasets (section S1), calibration of the glider data against CTD samples (section S2), and non-photochemical quenching correction (section S3).

2.2. Glider-derived primary production estimates

Glider-derived PP values were computed following the approach of Mignot et al. (2018) for biogeochemical-Argo data. This approach uses a bio-optical model to estimate daily-averaged, depth-integrated rates of PP based on glider vertical profiles of temperature, light, and chlorophyll concentration, as well as two prescribed photosynthesis parameters. The model resolves the daily time dependence of sea surface incoming solar radiation but it assumes that mixed layer depth, light attenuation coefficient (K), and chlorophyll concentration are constant during a single day. The two photosynthesis parameters are the chlorophyll-specific initial slope of the photosynthesis-irradiance curve, α^B (mgC mgChl^{-1} s^{-1}/μmol photons m^{-2} s^{-1}) and the maximum chlorophyll-specific light-saturated photosynthesis P^b_{max} (mgC mgChl^{-1} s^{-1}), which is calculated as an exponential function of P^b_{max} at 20 °C and the mixed layer-averaged potential temperature with a Q_{10} of 2. Based on *in situ* shipboard ^{14}C incubations, α^B is set to 11.67*10^{-6} (mgC mgChl^{-1} s^{-1})/(μmol photons m^{-2} s^{-1}) and P^b_{max} (20 °C) is set to 0.45*10^{-3} mgC mgChl^{-1} s^{-1}. Finally, the depth integration is performed
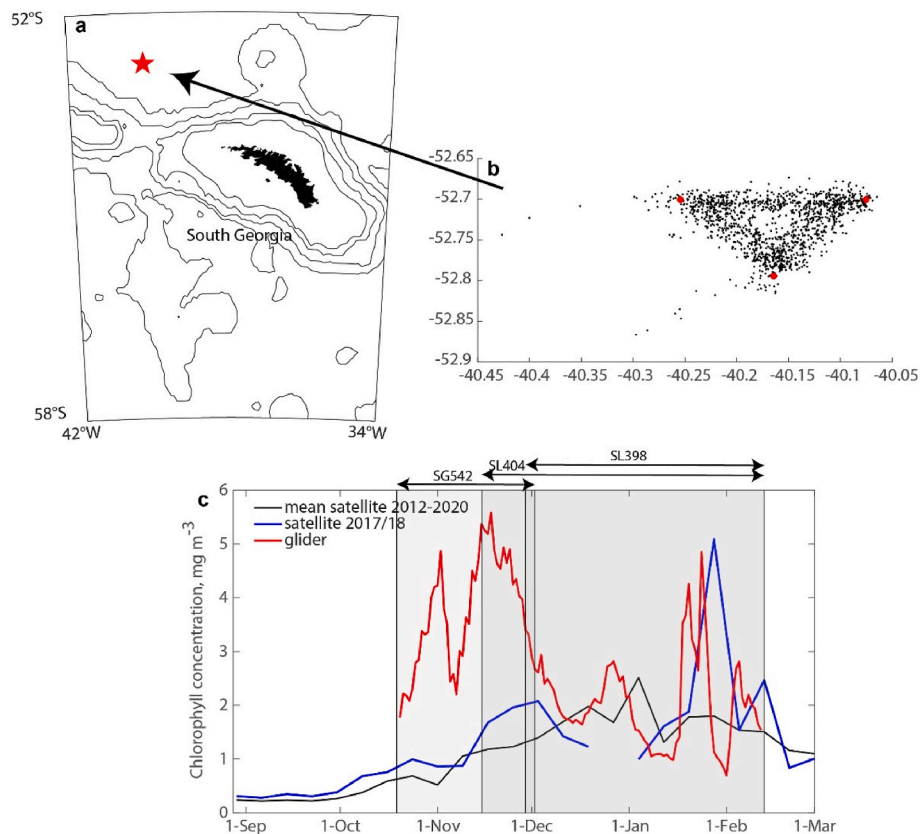
Fig. 1. a) Region of study area in the vicinity of South Georgia, Southern Ocean. Contours mark depths of 500, 1000, 2000, and 3000 m. Red star marks the location of the glider survey. b) Close-up of study region showing the locations of each glider surfacing in the period 19th October 2017–13th February 2018. Red dots mark the nominal glider waypoints at the corners of the survey triangle. c) Glider-derived chlorophyll concentration in the 5–10 m depth bin (red line), satellite chlorophyll data (MODIS-AQUA 4 km, 8 day resolution) for 2017–2018 (blue line) and the climatological mean of 2012–2020 (black line). Shading and arrows represent the deployment and recovery times of the 3 gliders used in this study.

over the greater of the mixed layer or the euphotic layer depth, where the euphotic layer depth is computed as -log(0.01)/K. We determined the uncertainty in our PP estimates by using the standard deviation in P_{max}^b and α^B measured during the cruise (n = 9), which produced an uncertainty in PP of ±40%. We nevertheless suggest that our approach results in less uncertainty than using satellite-derived PP estimates (the

only other means of assessing time-resolved variability in PP). Satellite-based estimates use only surface data and global photosynthetic parameters, whereas we are able to use full profiles of *in situ* glider data and regional photosynthetic parameters. Additionally, the temporal variability in the uncertainty estimates varied only fractionally (±1%) and so we conclude that the variations in PP are independent of
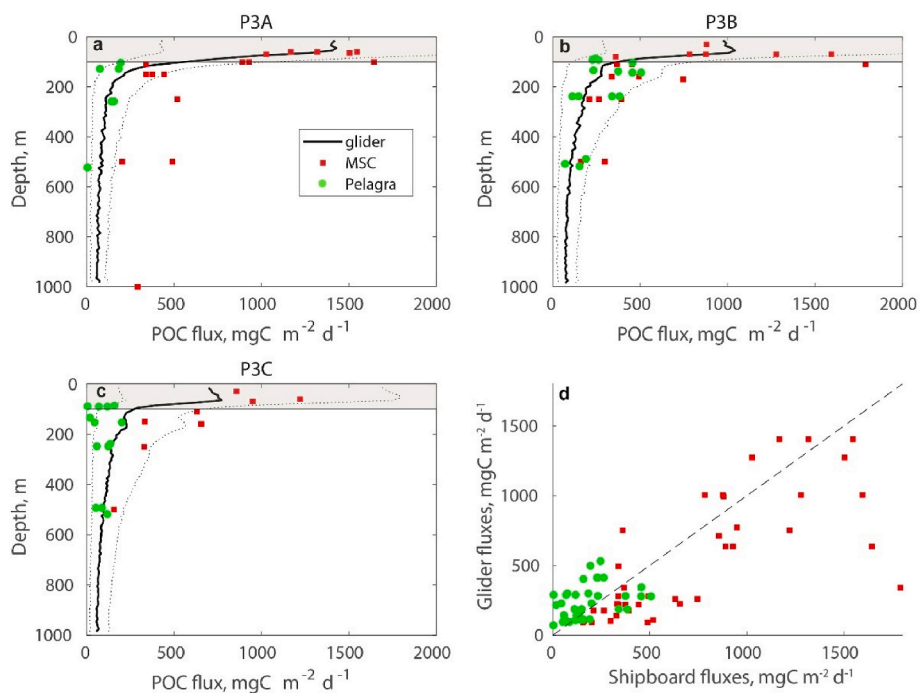

Fig. 2. a-c) Comparison of shipboard flux profiles measured by Marine Snow Catcher (MSC; red squares) and neutrally-buoyant sediment trap (Pelagra; green dots) deployments, and glider-derived profiles of flux averaged for the 3 site visits (black lines; P3A: 14–21 November 2017, P3B: 28 November-4 December 2017, P3C: 8–14 December 2017). Upper and lower uncertainty bounds on glider-derived fluxes are shown with dotted lines (see section 2.3 for definition). Glider-derived fluxes have greater uncertainty in the upper 100 m and so are shaded in grey. d) Scatter plot of all co-occurring shipboard and glider fluxes, with 1:1 line marked with a dashed line (linear regression statistics: r = 0.35, p < 0.01, n = 75, slope = 0.96, intercept = 92.1). See section 2.3 for details of glider calculations, and Giering et al. (this issue) for shipboard POC flux measurements.

the uncertainties in the terms of the phytoplankton growth model (Mignot et al., 2018). We therefore consider the relative changes in PP over time to be robust.

2.3. Glider-derived POC flux estimates

Total POC concentration, derived from an empirical relationship with backscatter (Supplementary Material section S2), was split into contributions from large and small fractions following the methods of Briggs et al. (2020, 2011). The small-particle POC is the $b_{bp}700$ "baseline" signal, whereas the large-particle POC is derived from the "spike" signals of all backscatter wavelengths (Supplementary Material section S4). Small-particle POC was bin averaged into two-day, 10 m bins to match large-particle POC. For each size class, flux was estimated as the product of POC concentration and bulk sinking speed (see section S4.3 for sinking speed estimates). Total POC flux was then estimated as the sum of small-particle POC flux and large-particle POC flux.

Uncertainty estimates in POC flux (shown as horizontal bars in Fig. 2) arise from the range in fast and slow sinking speeds used. The small-particle sinking speed was set to 0, 2.5 or 10 md^{-1} (Bannon and Campbell, 2017; Briggs et al., 2020) for the lower, central and upper bounds, respectively. For the large-particle fraction, a depth-varying sinking speed was derived from tracking pulses of material (Briggs et al., 2011, 2020; see section S4.3 in Supplementary Material). Sinking speed increased from ~70 md^{-1} at 100 m depth to ~130 md^{-1} at 900 m depth (Fig. S4; Villa-Alfageme et al., this issue). The central and upper uncertainty bounds shown in Fig. 2 use the sinking speeds shown in Fig. S4, and the lower bound estimate is calculated by halving these speeds to match camera-derived sinking speeds from the Pelagra deployments (Iversen, 2003).

The uncertainty estimates on the glider-derived POC fluxes (Fig. 2) reflect the large *a priori* uncertainty in the mean sinking speeds of particles in our two operationally-defined size classes (section S4.3). Our absolute values of POC flux should therefore be interpreted with caution, especially outside the cruise period, when calibration against ship-deployed instrumentation was not possible. However, the shipboard data do not suggest any consistent bias in our autonomous POC flux estimates at any time or depth (Fig. 2). Furthermore, the observation of coherent, discrete sinking particle plumes (Fig. S3) demonstrate that the gliders observed the same particle populations at different depths and times. Although potential changes in particle communities outside of the cruise period do add greater uncertainty to our absolute POC fluxes and the resultant export ratio at the beginning and end of our glider timeseries, nevertheless we expect our observed trends in T_{eff}, S_{eff}, and M_{eff} to be robust to any variation in POC:bbp ratio or sinking speed because these variations are likely to propagate to depth as the particles sink. Therefore, our absolute POC flux estimates are likely to be good first-order quantitative estimates and, most significantly for the focus of this manuscript, the relative changes with depth and time (used to calculate changing export and transfer efficiencies) are robust and informative, despite the uncertainty in individual POC flux estimates.

2.4. Comparison of glider and shipboard flux data

The glider-derived POC flux is compared to shipboard Marine Snow Catcher and neutrally-buoyant sediment trap (Pelagra) flux data in Fig. 2. For details of the shipboard measurements, see Giering et al. (this issue). The glider-derived profiles of POC flux are consistent with the MSC-derived fluxes (r = 0.74, p < 0.001, n = 40, slope = 0.68), although the MSC data are instantaneous snapshots of flux and the glider data are averaged over each sampling epoch (7–8 days). The Pelagra-derived fluxes tended to be somewhat lower than the MSC and glider fluxes, particularly for P3C (correlation between Pelagra and glider fluxes: r = 0.36, p = 0.03, n = 35, slope = 0.34). However, the conical-shaped Pelagra traps have been found to undertrap small particle fluxes relative to cylindrical traps in an intercomparison study (Baker et al., 2020).

As an additional constraint on our glider-derived fluxes, our 1000 m glider-derived fluxes were compared to fluxes from a deep moored sediment trap at 2000 m depth. The deep moored sediment trap was deployed at P3 at 52.72 °S, 40.16 °W in December 2016 from the *RRS James Clark Ross*. The sediment trap carousel was programmed to rotate every 5 days between mid-October 2017 and late January 2018, i.e. for much of the glider deployment period. Full details of the sediment trap deployment, methodology and deep flux data can be found in Manno et al. (2022). The fluxes at 2000 m depth are consistently lower than our 1000 m fluxes, as expected (see Results section), providing further confirmation that our glider-based flux estimates are in a realistic range.

2.5. Potential influence of advection on glider time series

The gliders followed a set triangular path around the study location (Fig. 1b) and as such were sampling in a Eulerian, rather than Lagrangian, frame. Although the study location was specifically selected for its quiescence, the possible influence of lateral advection nonetheless needs to be assessed. The glider deployments were located in the Georgia Basin between the Polar Front (to the north) and the Southern Antarctic Circumpolar Current Front (to the south) (Owens et al., 2015; Venables et al., 2012), and within a retentive circulation, notable for its low current speeds and weak mesoscale activity (Brandon et al., 2000; Matano et al., 2020; Meredith, 2003). Satellite-derived surface current speed data (https://podaac.jpl.nasa.gov/dataset/OSCAR_L4_OC_third-deg; Fig. 3a) confirms that despite some variability the gliders experienced relatively low current speeds for the duration of the deployment (<0.06 m s^{-1}). The ship-board ADCP data confirms that these weak current speeds extend into the mesopelagic (Fig. S6). However, starting from ~1 January 2018, an unusually sustained period of relatively fast, north-westward currents (Fig. 3a) is evident. This period coincides with anomalies in satellite chlorophyll data with respect to the multi-year climatology (Fig. 1c), with both the satellite and glider chlorophyll concentration exceeding the long-term mean from mid-January to mid-February by ~ 3 mg m^{-3}. A relatively clear satellite image from 16 January 2018 highlights the patchy nature of the spatial distribution of chlorophyll around the glider study site during this period (Fig. 3b), ranging from 1 to 10 mg m^{-3} over small distances (of note is the high chlorophyll region immediately to the south of the glider study). The individual chlorophyll measurements recorded within the top 25 m during each glider dive plotted in Fig. 3c and d shows advection of high chlorophyll waters from the south into the glider sampling region. Another period of relatively high northwestward current speeds (and peak in chlorophyll) occurs during 2–6 February. The potential influence of advection during these periods needs to be taken into consideration, in particular when comparing deep fluxes to export fluxes, as the source region of the particles could be more distant from the sampling location at greater depths (Siegel and Deuser, 1997). If upper ocean export is spatially patchy, the particles sampled at depth may therefore not reflect the conditions in the immediate vicinity of the glider sampling triangle. However, outside of the periods identified above, no evidence of strong lateral advection was observed in the remainder of the dataset and we therefore interpret it principally as a time series. It should nevertheless be noted that even weak horizontal currents can result in particles at depth originating a considerable lateral distance away from the sampling region. In our case, assuming that the surface currents shown in Fig. 3a (on the order of ~3.5 km d^{-1}) remain constant with depth and an average sinking speed of ~100 md^{-1}, particles reaching the trap at 2000 m depth could have originated from up to 70 km away.

2.6. Definition of flux and efficiency terms

The depth of export is defined here as the base of the productive layer (Z_p), which we define operationally as the deepest depth at which chlorophyll exceeds 10% of its maximum for each individual profile,
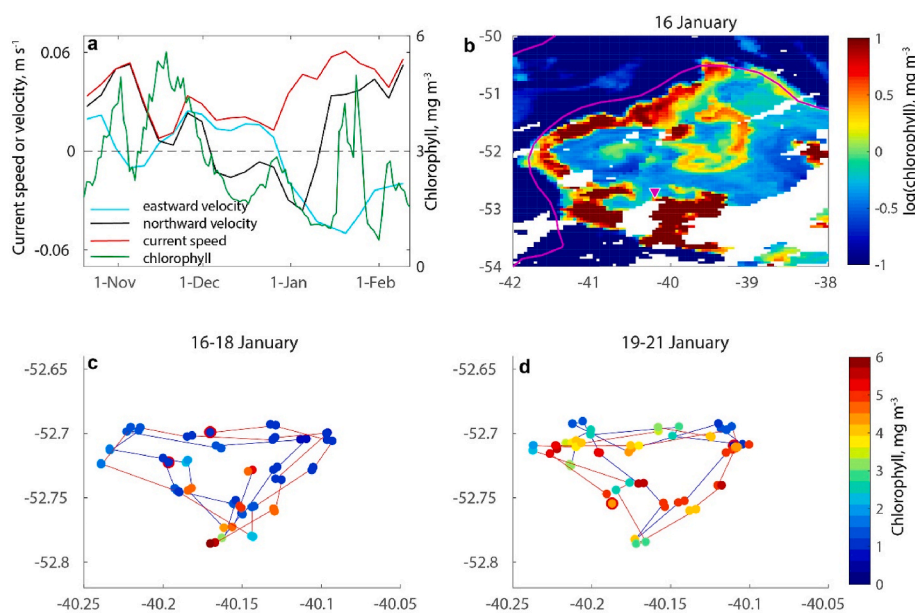
Fig. 3. a) Current speed (red) and zonal and meridional velocities (cyan and black, respectively) from OSCAR satellite product, and the glider-derived time series of chlorophyll at 15 m depth (green), b) combined MODIS-Aqua and MODIS-Terra satellite log (chlorophyll concentration) image from 16th January 2018; study site is marked with a magenta triangle and southern boundary of the Polar Front is marked with a pink contour (Venables et al., 2012); c-d) individual glider profile chlorophyll concentration averaged over 0–25 m depth showing likely lateral advection event from 16 to 21 January 2018; the path of SL398 (SL404) is marked with a blue (red) line, with the first profile of each period outlined by a red ring.

following Owens et al. (2015). Our Z_p value is never shallower than a conservative euphotic depth estimate (depth where $PAR_z = 0.1\% * PAR_0$), and matches or exceeds the seasonal mixed layer depth (defined as 0.05 kg m^{-3} density difference from surface values) throughout the study period, with a median difference of 19 m. Export flux is defined as flux at Z_p, mesopelagic flux is defined as flux at Z_p+100 m, sequestration flux is defined as the flux averaged in the depth range 900–1000 m, and the deep flux comes from a moored sediment trap at 2000 m depth. Export efficiency is defined as flux at Z_p/PP, transfer efficiency (T_{eff}) is defined as flux at Z_p+100 m/flux at Z_p, sequestration efficiency (S_{eff}) is defined as flux averaged in the depth range 900–1000 m/flux at Z_p, mesopelagic efficiency (M_{eff}) is defined as flux averaged in the depth range 900–1000 m/flux at Z_p+100 m, and the deep flux efficiency (D_{eff}) is defined as flux at 2000 m/flux averaged in the depth range 900–1000 m.

3. Results

Satellite data spanning the period before the glider deployment suggests that chlorophyll concentration was increasing gradually during September and early October 2017 (Fig. 1c). The ~4 month glider deployment captured the majority of the seasonal bloom, including the ramp up to the seasonal peak and subsequent decline into a series of smaller blooms.

The daily-averaged, 1 m depth resolution timeseries of temperature, oxygen, chlorophyll and POC concentration from the entire 4 month deployment is shown in Fig. 4, along with the monthly-mean profiles. Equivalent plots for potential density and apparent oxygen utilisation are in Fig. S5. The temperature profiles show the expected seasonal increase in upper ocean temperature, and a clear signature of the previous winter's remnant mixed layer, formed by deep convection (Meredith, 2003; Mosby, 1934). The oxygen data (Fig. 4b) show a decrease in upper ocean dissolved oxygen concentration during the course of the deployment (despite enhanced biological activity), demonstrating the dominance of seasonal heating-driven outgassing of oxygen (Verdy et al., 2007). The chlorophyll timeseries (Fig. 4g) shows an increase in productive layer concentrations from October through November, followed by a gradual decline until the end of the deployment in February (except for the 2 periods of lateral advection identified in section 2.5). POC concentration follows a similar pattern (Fig. 4h), increasing in the upper ocean in October and November, before declining (again excluding potential advective periods). Of note in the timeseries of both

chlorophyll and POC concentration are periods (notably from the end of November to early January) in which elevated particle concentrations occur below the productive layer, reaching depths of 400–500 m (Fig. 4c and d), suggesting that fresh material is being exported into the upper mesopelagic without undergoing remineralisation in the upper ocean, and/or *in situ* particle fragmentation is occurring.

The export flux from the base of the productive layer reveals considerable temporal variability on timescales of days to months (Fig. 5b). During the initial bloom (start of time series to ~ 1 December), the export flux remains high, although with daily variability superimposed, then declines after the bloom peak. Pulses of elevated export flux lasting ~1 week occur post-bloom in concert with pulses of elevated PP. The flux 100 m below the productive layer depth (here termed the 'mesopelagic flux'; Fig. 5c) mirrors the export flux through mid-December, albeit with a slightly later peak. After mid-December, mesopelagic flux displays little variability, in contrast with the three pulses apparent in PP and export flux. The sequestration flux (flux average at depths 900–1000 m; Fig. 5d) increases very gradually until early December with a lag of ~15 days with respect to PP and export flux, and thereafter declines slowly. The deep flux, captured by a moored sediment trap at 2000 m depth, has three distinct peaks (Fig. 5e): one pre-bloom peak, one post-peak and one in the decaying phase of the bloom (Manno et al., 2022), superimposed on a pattern of increase and decline similar to sequestration flux.

The temporal variability in the fluxes is naturally reflected in significant variability in the flux ratios. The export efficiency declines during the bloom onset phase until the bloom peak (i.e. to mid-November) and thereafter is fairly constant (Fig. 5f). Transfer efficiency from Z_p to Z_p+100 m in contrast increases gradually from a minimum at the beginning of the time series to a peak in late January (Fig. 5g). During the bloom growth phase, T_{eff} remains at moderate values, with only relatively small temporal variability. However, after the bloom peak T_{eff} varies more substantially around a higher mean, with peaks occurring during low PP periods. The sequestration efficiency behaves similarly to T_{eff} with a fairly constant value during the bloom phase, and an increased mean and temporal variability post-bloom peak (Fig. 5h). Again, periods of peak S_{eff} correspond to periods of low PP. However, the mesopelagic efficiency shows opposing trends to T_{eff} and S_{eff}, with, on average, higher values occurring in the bloom growth phase than post-bloom (Fig. 5i). Finally, the deep flux efficiency shows pulses of substantially higher D_{eff} (Fig. 5j), coincident with higher deep flux episodes.
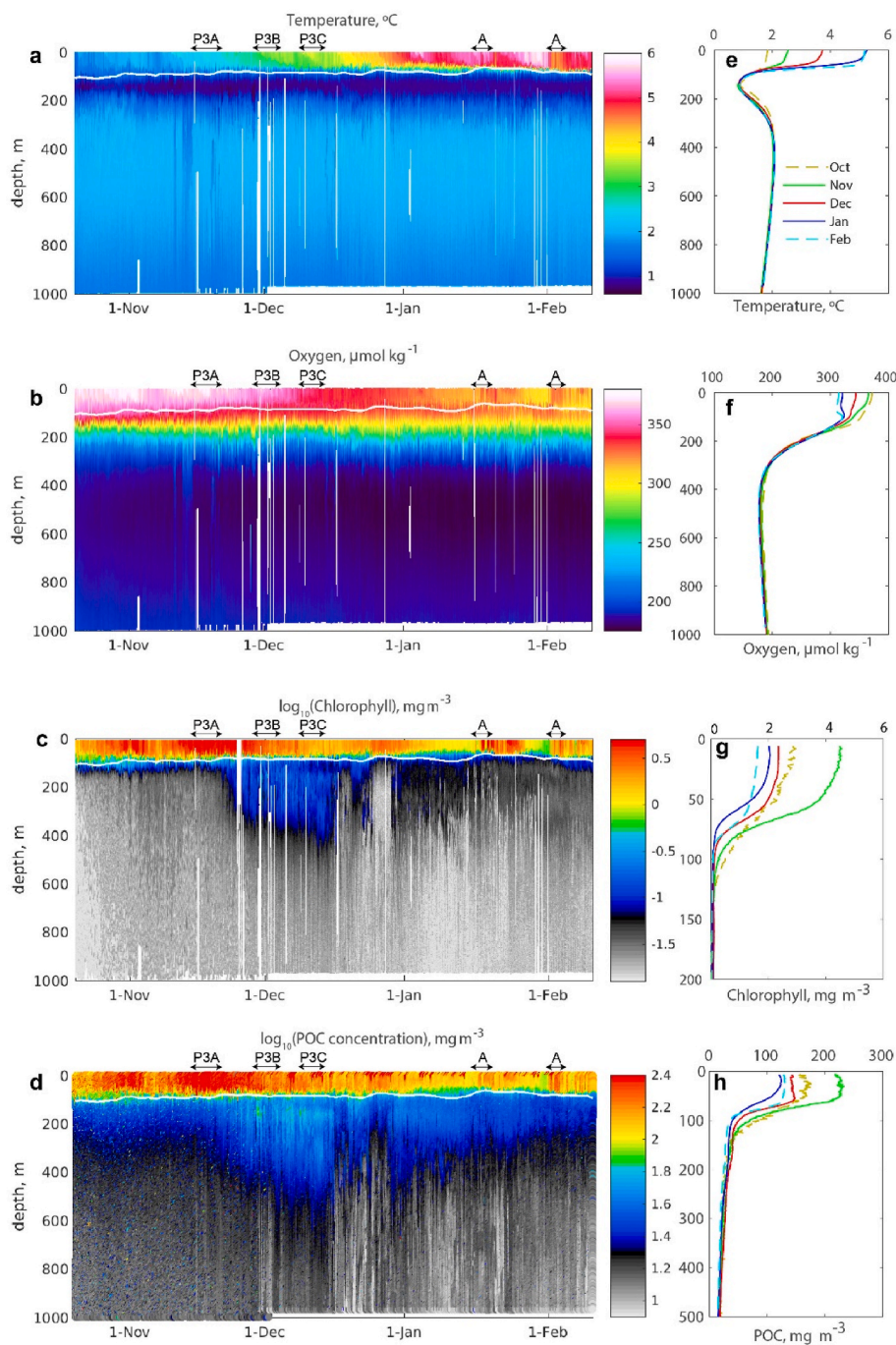
Fig. 4. Daily, 1 m vertical resolution data for the full glider deployment for a) temperature, b) oxygen concentration, c) log(chlorophyll concentration) and d) log(POC concentration). The white line represents the productive layer depth (see section 2.6 for definition). The 3 cruise sampling epochs are labelled (P3A, P3B and P3C), as are two periods of potentially enhanced lateral advection (marked A; see section 2.5). Right column shows monthly mean vertical profiles of e) temperature, f) oxygen concentration, g) chlorophyll concentration and h) POC concentration. October and February are plotted as dashed lines as there is only partial data in those months (13 days in both). Note the change in vertical scale in plots g) and h).

4. Discussion

4.1. Temporal variability in biological carbon pump magnitude and efficiency

The Southern Ocean is a region of strongly seasonal biomass production and associated carbon export. The organic material exported by the annual bloom is likely to play a significant role in ocean carbon uptake and biogeochemical cycling (Marinov et al., 2006; Uchida et al., 2019), particularly in high productivity, iron-fertilised regions, such as downstream of South Georgia. The glider deployments presented here were able to capture the majority of the seasonal bloom, including high resolution characteristics of primary production and sinking flux during the bloom growth phase and subsequent decline over a 4 month period,

revealing substantial temporal variability in both POC flux magnitude and efficiency on timescales of days to months.

In the first ~3 weeks of the glider time series, PP increases while export flux is already relatively high (Fig. 5a and b), leading to declining export efficiency. In the post-bloom peak phase, the PP and export flux vary in sync such that the export efficiency has relatively low temporal variability (Fig. 5f). The combination of our high export efficiency estimates and net productive layer POC accumulation (Fig. 4d) during the early bloom phase imply minimal heterotrophic POC consumption. These results echo findings using similar autonomous methods in the springtime North Atlantic, which also suggested that heterotrophic respiration was a minimal fraction of PP in the early spring bloom period and a high fraction of PP during and after the bloom decline (Briggs et al., 2018). The high export efficiency in the early bloom phase is
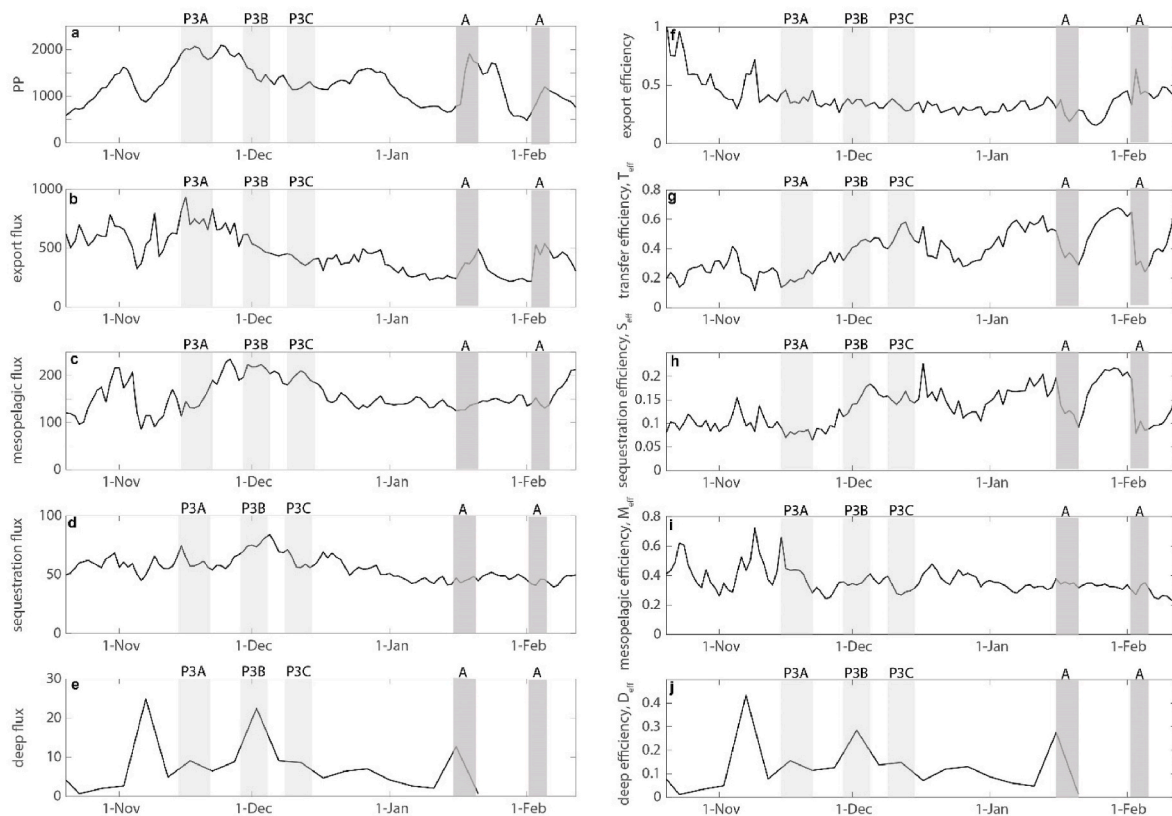
Fig. 5. Time series of glider-derived a) primary production, b) export flux at the productive layer depth (Z_p), c) mesopelagic flux (flux at depth of $Z_p + 100$ m), d) sequestration flux (flux averaged in the depth range 900–1000 m), and e) deep flux collected by a moored sediment trap at 2000 m depth (from Manno et al., 2022), all in mg C m^{-2} d^{-1}. Time series of glider-derived f) export efficiency (export at Z_p/PP), g) transfer efficiency (T_{eff}; flux at $Z_p + 100$ m/flux at Z_p), h) sequestration efficiency (S_{eff}; flux averaged over 900–1000 m/flux at Z_p), i) mesopelagic efficiency (M_{eff}; flux averaged over 900–1000 m/flux at $Z_p + 100$ m), and j) deep efficiency (D_{eff}; flux at 2000 m/flux averaged over 900–1000 m). The 3 cruise sampling epochs are labelled (P3A, P3B and P3C), as are two periods of potentially enhanced lateral advection (marked A; see section 2.5).

consistent with our conceptual understanding of bloom dynamics, i.e. at the start of the growing season, phytoplankton are likely to be able to outpace their grazers who have slower growth rates and as a result, productivity may become decoupled from upper ocean remineralisation processes allowing high export efficiency to occur (Baumann et al., 2013; Buesseler and Boyd, 2009; Henson et al., 2019).

During the bloom ramp-up and peak phases, export efficiency declines as T_{eff} and S_{eff} begin to increase. Coincident data from the COMICS1 cruise found abundant heavily silicified live diatoms in the mesopelagic, suggesting direct sinking of cells without significant reworking in the upper ocean (Ainsworth et al., 2023). This is consistent with the composition of deep fluxes which consisted mainly of intact diatom cells during the bloom ramp-up phase (Manno et al., 2022). Furthermore, high chlorophyll concentrations observed below the productive layer in December (Fig. 4c) are also indicative of relatively fresh material sinking into the upper mesopelagic, perhaps as aggregates that then fragment into smaller, slower sinking particles (Briggs et al., 2020). Taken together, these results suggest that the aggregates formed during this period may have been particularly fragile, leading to lower export efficiency during the bloom peak (relative to the bloom growth phase).

As the bloom developed towards its peak, the composition of deep fluxes shifted to partially grazed phytodetritus (Manno et al., 2022) which implies that the mesopelagic zooplankton community were unable to process the influx of particles during the bloom peak, either because the generation time of the recycling organisms is too long to be able to respond sufficiently rapidly to a sudden increase in food supply and/or because particles sink too rapidly to be fully remineralised in the mesopelagic. A particular region or system may therefore have a maximum capacity to consume/recycle POC; if the incoming flux

exceeds that capacity, 'leakage' of POC to deeper depths occurs. These POC pulses may transit all the way to the seafloor, thus contributing to long-term ocean carbon storage (e.g. Cartapanis et al., 2016). Episodic depositions of organic material are known to occur (e.g. Billett et al., 2010; Rembauville et al., 2015) and may at times even be sufficient to sustain the benthos (Smith et al., 2013).

During the declining bloom phase, export efficiency is relatively constant (Fig. 5f), implying a tight coupling between PP and export production, with phytoplankton growth and zooplankton grazing acting in sync. The seasonally changing degree of (de)coupling between PP and export highlighted in our multi-month glider data is in contrast to model-based estimates, which suggest that the lag between PP and export at high latitudes is ~15–30 days (Henson et al., 2015). The single lag calculated for a climatological year of monthly PP and export in the model study of Henson et al. (2015) is most likely an oversimplification of the dynamic nature of export processes and subsequent fluxes. Indeed, both T_{eff} and S_{eff} show greater variability than export efficiency and remain high, relative to the bloom growth phase. The deep flux was dominated by mostly intact diatom resting spores during the bloom decline (Manno et al., 2022), implying that these particles are less labile or have greater sinking speeds than the aggregates and fecal pellets generated in the earlier phases of the bloom.

The time series of T_{eff} and M_{eff} (i.e. upper mesopelagic and lower mesopelagic efficiency, respectively; Fig. 5g,i) have opposing trends, with T_{eff} increasing post-bloom peak and M_{eff} decreasing. These patterns imply that the majority of remineralisation occurs in the upper 100 m below the base of the productive layer in the early phases of the bloom, before concentrating deeper in the mesopelagic in the post-peak phase. The fluxes (and by association the particle remineralisation processes) in

the upper and lower mesopelagic are thus somewhat disconnected, i.e. an increase in flux at 100 m below the productive layer doesn't necessarily translate to an increase in flux at 1000 m, or 2000 m, depth. This disconnect could be influenced by lateral advection introducing particles that have originated from a remote location, particularly in the latter part of our dataset where two advection events are identified (see Section 2.5 and Fig. 3). Additionally, the disconnect between upper ocean and deep fluxes could reflect a vertical structure in the prevailing particle type, size and/or remineralisation process, which furthermore also have different seasonal trends. For example, labile particles may be reworked by zooplankton activity in the upper mesopelagic transitioning to a dominance of relatively refractory particles being remineralised by bacteria in the lower mesopelagic (Iversen, 2003), combined with stronger seasonal variability in zooplankton populations than bacteria. Alternatively (or additionally), the particle size spectrum may change with depth, as particles get fragmented into smaller, potentially slower sinking, particles (Baker et al., 2017; Briggs et al., 2020). Given this apparent disconnect between temporal trends in upper and lower mesopelagic fluxes, calculating a single remineralisation length scale or "Martin's b" (Martin et al., 1987) for the entire water column may not reflect the attenuation occurring over different depth ranges (Cael and Bisson, 2018).

Our results complement the handful of other studies that have examined temporal variability in export efficiency and transfer efficiency, either from autonomous vehicles, mesocosm studies, or repeat shipboard visits. These studies reach contrasting conclusions about the seasonal progression of export efficiency and flux attenuation. In contrast to our results, Briggs et al. (2018) found that, in the North Atlantic, export efficiency was low in the early bloom phase, increased during the bloom peak and decline, and then dropped significantly in the post-bloom period. Our findings also differ from Baumann et al. (2013), who found low springtime export efficiency followed by higher values in the summer in the Bering Sea. However, our analysis is consistent with glider observations over a full year in the Northeast Atlantic, which revealed that T_{eff} was at its minimum during the bloom period (Bol et al., 2018). On the other hand, in the subtropical Atlantic, profiling floats equipped with optical sediment traps revealed that flux attenuation was lower (i.e. high T_{eff}) during the bloom than before or after it (Estapa et al., 2019), in contradiction to mesocosm experiments in the subtropical Atlantic which demonstrated a higher flux attenuation (i.e. low T_{eff}) during the bloom peak (Bach et al., 2019). Using global data syntheses, both Lam et al. (2011) and Guidi et al. (2009) found that diatom blooms (i.e. typically high latitude regions) have high export efficiency, but low T_{eff}, whereas regions dominated by smaller phytoplankton types (i.e. typically low latitudes) experienced the reverse. The opposing situation in subtropical and subpolar regions suggests that the differing ecosystem structures typical of these areas result in differing responses to periods of high flux. However, more direct observations of temporal variability in fluxes is needed to ascertain whether these patterns are applicable on global scales.

4.2. Drivers of temporal variability in flux attenuation

Three primary hypotheses currently exist to explain patterns in flux attenuation: temperature, oxygen concentration, and community structure (Sanders et al., 2016). Temperature has been shown to be a useful correlate for global scale spatial variability in flux attenuation (Cram et al., 2018; Dunne et al., 2005; Henson et al., 2012a; Marsay et al., 2015). Spatial gradients in temperature are large across the global ocean, and temperature is a useful first order indicator of productivity in a region, i.e. cooler regions tend to be more productive than warmer ones (e.g. Longhurst, 2006). As a result, correlation of temperature with flux attenuation in global data compilations is perhaps unsurprising. The question remains however whether the observed correlation between flux attenuation and temperature is causative. There are solid mechanistic grounds to expect temperature to be important in controlling flux

attenuation via its central role in setting metabolic rates, including respiration (e.g. Boscolo-Galazzo et al., 2018). However, here we find that flux attenuation (represented by S_{eff}) varies between 0.06 and 0.23 during the course of the bloom. This is roughly half of the entire global range (0–0.4; Cram et al., 2018; DeVries and Weber, 2017; Henson et al., 2012a; Weber et al., 2016) within a single seasonal cycle – a phenomenon also noted by Buesseler and Boyd (2009) and Lam et al. (2011). Furthermore, during our glider deployments, the mean temperature between 0 and 500 m (as used in Marsay et al. (2015) to define ambient temperature) varied by only 0.4 °C around its median value of 2 °C. With a typical Q_{10} value of 2, this temperature variation implies a mere 3% change in remineralisation rate. Variability in temperature is therefore not driving the substantial temporal variability in flux attenuation. The same is likely to be true of most open ocean locations: seasonal subsurface temperature changes are typically small, and therefore temperature cannot be the primary driver of local or temporal variability in BCP efficiency. However, it is nevertheless a good proxy for describing differences in BCP efficiency across a wide dynamic range of temperatures, such as when comparing ocean basins or disparate sites.

Mesopelagic oxygen concentration has also been suggested as an important factor affecting sequestration efficiency (Cavan et al., 2017; Devol and Hartnett, 2001). However, this effect is likely only of relevance in low oxygen zones (Cram et al., 2018), whereas at our Southern Ocean site, oxygen concentration remains well above suboxic levels throughout the year.

Alternatively, community structure has been hypothesised as a control on flux attenuation (Boyd and Newton, 1999; Henson et al., 2012a; Lima et al., 2014; Wiedmann et al., 2020). The COMICS1 cruise data span only a short period of our glider dataset, but nonetheless suggest that neither the phytoplankton or zooplankton community structure changed significantly between mid November and mid December, although overall phytoplankton biomass declined (Cook et al., this issue; Ainsworth et al., 2023). It remains unclear then how, or whether, changing community structure played a role in driving temporal variability in flux attenuation during the glider deployment. Potentially, the range in typical local temperature sets the maximum possible metabolic rate for a particular location, while seasonal variability in flux attenuation is controlled by the local ecosystem state. An additional consideration is that community structure should not be considered as a control on flux attenuation in isolation, as it is not independent of temperature and oxygen concentration, with both zooplankton and microbial activity responding to changing environmental conditions. Community structure encompasses a myriad of different possible processes – not just changes to the abundance of dominant taxa, but also how that alters production of transparent exopolymers, fragmentation, aggregation, particle sinking speed, fecal pellet morphology, particle lability, viral lysis and many more factors (e.g. Cavan et al., 2019; Passow and Carlson, 2012). 'Community structure' is thus a convenient catch-all which, arguably, does little to advance a mechanistic understanding of controls on flux attenuation.

4.3. Influence of temporal variability on interpretation of flux observations

The high resolution glider dataset allows POC fluxes to be examined on multiple time scales. In Fig. 6 for example, the monthly mean, 2-week running mean, and daily data are plotted, revealing a monthly scale pattern of declining export efficiency and increasing transfer efficiency as the bloom peaks and declines, as well as the daily episodicity of the fluxes. The fraction of PP reaching 100 m below the export depth (contours in Fig. 6) can vary from ~0.05 to 0.3 in the space of a week, implying that flux to the mesopelagic is highly episodic. The episodicity and rapid variability in export efficiency and T_{eff} revealed in our high resolution datasets is unlikely to be resolved by typical shipboard deployments for flux studies, e.g. Marine Snow Catchers or neutrally buoyant sediment traps, for which typical sampling periods range from
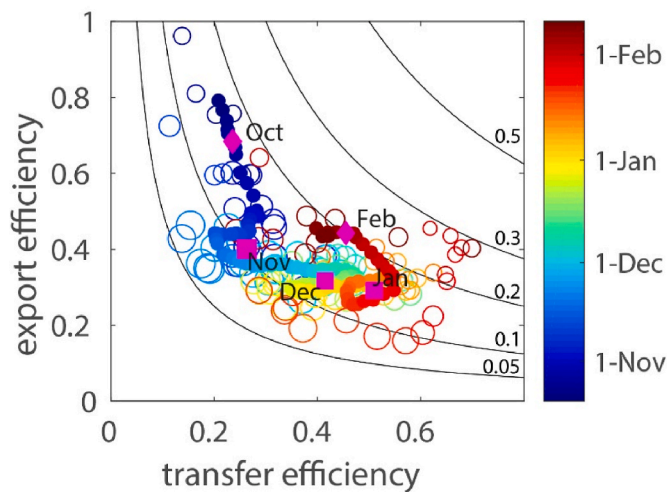
Fig. 6. Daily values of export efficiency plotted against transfer efficiency (flux at $Z_p + 100$ m/flux at Z_p) in open circles, where the size of the circles is scaled to primary production and colour indicates day of year. Filled dots are the 14-day running mean of export efficiency and transfer efficiency. The monthly mean values are plotted in pink diamonds for partial months (October and February, 13 days each) and in pink squares for full months (November, December and January). Contours indicate the ratio of flux at $Z_p + 100$ m to primary production.

instantaneous to a couple of days. The community's reliance, until recently, on discrete shipboard sampling to obtain export flux or mesopelagic flux attenuation data may bias interpretation of the flux patterns and therefore its potential drivers.

As an example, a shipboard profile of flux was collected using Marine Snow Catchers (Giering et al. this issue) on 5th December 2017 (during epoch P3B), for which T_{eff} was estimated at 0.48 (glider-based estimate is 0.45 on this date). Based on the instantaneous *in situ* data alone, we might conclude that fairly strong attenuation of flux occurs in the upper mesopelagic during the post-peak bloom phase in the South Georgia region. However, the daily glider data reveal a much more nuanced pattern during December, with daily T_{eff} values varying between 0.28 and 0.58. Extending this analysis, if the cruise-period glider-derived mean export efficiency value (0.35) is applied to time-integrated satellite-derived PP (analogous to the approach of e.g. Ceballos-Romero et al., 2016; Fan et al., 2020; Henson et al., 2011), the total cruise-period export flux is estimated as 9 gC m^{-2}. Applying the cruise-period mean sequestration efficiency (0.12) then results in an estimated total flux to 1000 m of 1.1 gC m^{-2}. The assumption of time-invariant export and sequestration efficiency results in substantial underestimates of the actual cruise-period total export and sequestration fluxes, which the glider is able to resolve. In this case, export flux is underestimated by 49% (actual flux = 17.8 gC m^{-2}) and sequestration flux by 45% (actual flux = 2 gC m^{-2}).

This example demonstrates a limitation of quasi-instantaneous shipboard flux data: the difficulty of determining whether a particular deployment has sampled an extreme in conditions, or whether the data collected are representative of that location and season. Generally, it is necessary to make the assumption that typical conditions have been sampled due to an absence of data on the seasonal range of conditions for a region. However, inadvertently sampling extremes may have distorted our view on the typical range in BCP magnitude and efficiency for a region, how those might change seasonally, and what the possible drivers of the BCP may be. As the example above shows, assuming a time-invariant efficiency or that a single sample is representative of the mean, can result in significant discrepancies between actual and estimated fluxes. Syntheses of shipboard flux data designed to deduce global-scale patterns of BCP flux or efficiency (e.g. Le Moigne et al.,

2013; Mouw et al., 2016) also suffer from potential biases due to the limited temporal coverage and/or resolution of the observations (as well as biases in spatial coverage), and the necessary assumption that representative conditions have been sampled. These data syntheses are frequently used to deduce global spatial patterns in BCP magnitude or efficiency, potential mechanisms underlying those patterns, and to develop and validate global biogeochemical models (e.g. Crichton et al., 2021; Stock et al., 2020). Our lack of knowledge on temporal variability in flux on daily to seasonal timescales must inevitably introduce uncertainties into our conceptual understanding of the BCP, and thus how we parameterise mechanistic models and interpret their projections of contemporary and future BCP. To what degree the use of global shipboard data syntheses has affected our perspectives on the BCP is difficult to quantify, however as we demonstrate here, and has been observed previously (e.g. Lam et al., 2011), the range in BCP efficiency at one location within a bloom period can be equivalent to the entire global range.

5. Concluding remarks

Autonomous vehicle-derived estimates of particle fluxes offer unparalleled resolution over months or years, allowing the variability in the BCP to be quantified on temporal scales impossible to achieve with shipboard campaigns alone. Our dataset demonstrates that temporal variability is large, and occurs on multiple time scales from daily to seasonal. In this high productivity region, we find high export efficiency, but low transfer efficiency, during the bloom growth phase, while the peak bloom period is characterised by declining export efficiency, but increasing transfer efficiency. In the post-bloom phase, transfer efficiency increases in the upper mesopelagic, but decreases in the lower mesopelagic. Whether our results are more broadly applicable to other regions remains an open question. There are currently too few seasonally resolved observations of mesopelagic flux and efficiency to ascertain any significant global-scale patterns. However, we note that our results are consistent with analysis of glider data in another high latitude, seasonally variable region of the Northeast Atlantic (Bol et al., 2018). The opposite pattern, of higher transfer efficiency during the bloom period than outside it, was however observed in a subtropical, weakly seasonal region (Estapa et al., 2019). We await more seasonally resolved data to determine whether these patterns are typical for high and low latitude regions.

Syntheses of the sparse and biased (both spatially and temporally) shipboard observations of sinking flux (e.g. Le Moigne et al., 2013; Mouw et al., 2016) have, by necessity, been used to shape the community's concepts of the characteristics of the BCP. Parameterisations of the BCP for biogeochemical models have then been developed on the basis of the understanding drawn from shipboard data. However, the new insights starting to arise from autonomous vehicle observations emphasise the need to begin incorporating these findings on the magnitude and characteristics of temporal variability into our conceptual understanding of the BCP, and hence into new model developments. Additionally, biogeochemical model fields of POC flux or transfer efficiency are typically validated against either the sparse and biased shipboard data syntheses, or against satellite data-based global maps, themselves derived from the sparse shipboard datasets. The advent of temporally-resolved datasets of POC flux allows truly representative means on daily, weekly, monthly (or any other) timescale to be calculated, thus allowing a more robust comparison of model outputs and observations.

Despite the obvious advantages of autonomously-derived flux data, the drawback is the lack of information on processes underlying the observed variability. We speculate here on the possible drivers underlying the temporal variability, such as changing community structure, remineralisation rates etc., but we cannot go further than speculation. This highlights a current fundamental limitation of many autonomous observations of the BCP, although significant insights into some

mesopelagic processes from autonomous observations have been gained (e.g. Briggs et al., 2020). Ongoing technological developments, for example incorporating camera systems into autonomous vehicles (e.g. Lombard et al., 2019), have the potential to allow further insights into the processes driving variability in the BCP. Although significant technical challenges are associated with, for example, capturing rates (rather than states), characterising particle composition, the processing of terabyte-scale datasets, and interpretation of image data, the combination of novel sensors with autonomous platforms holds the promise to usher in a new era of BCP research.

Author statement

Declaration of competing interest

The authors declare that they have no known competing financial interests or personal relationships that could have appeared to influence the work reported in this paper.

Data availability

Data will be made available on request.

Acknowledgements

Appendix A. Supplementary data

Supplementary data to this article can be found online at https://doi.org/10.1016/j.dsr2.2023.105274.

References

Ainsworth, J., Poulton, A., Lohan, M., Stinchcombe, M., Lough, A., Moore, C.M., 2023. Iron cycling during the decline of a South Georgia diatom bloom. Deep Sea Res. II 208. https://doi.org/10.1016/j.dsr2.2023.105269.

Atkinson, A., Whitehouse, M., Priddle, J., Cripps, G., Ward, P., Brandon, M., 2001. South Georgia, Antarctica: a productive, cold water, pelagic ecosystem. Mar. Ecol. Prog. Ser. 216, 279–308. https://doi.org/10.3354/meps216279.

Bach, L.T., Stange, P., Taucher, J., Achterberg, E.P., Algueró-Muñiz, M., Horn, H., Esposito, M., Riebesell, U., 2019. The influence of plankton community structure on sinking velocity and remineralization rate of marine aggregates. Global Biogeochem. Cycles 33, 971–994. https://doi.org/10.1029/2019GB006256.

Baker, C.A., Estapa, M.L., Iversen, M., Lampitt, R., Buesseler, K., 2020. Are all sediment traps created equal? An intercomparison study of carbon export methodologies at the PAP-SO site. Prog. Oceanogr. 184, 102317 https://doi.org/10.1016/j.pocean.2020.102317.

Baker, C.A., Henson, S.A., Cavan, E.L., Giering, S.L.C., Yool, A., Gehlen, M., Belcher, A., Riley, J.S., Smith, H.E.K., Sanders, R., 2017. Slow-sinking particulate organic carbon in the Atlantic Ocean: magnitude, flux, and potential controls. Global Biogeochem. Cycles 31, 1051–1065. https://doi.org/10.1002/2017GB005638.

Bannon, CC, Campbell, DA, 2017. Sinking towards destiny: High throughput measurement of phytoplankton sinking rates through time-resolved fluorescence plate spectroscopy. PLoS One 12 (10), e0185166. https://doi.org/10.1371/journal.pone.0185166.

Baumann, M.S., Moran, S.B., Lomas, M.W., Kelly, R.P., Bell, D.W., 2013. Seasonal decoupling of particulate organic carbon export and net primary production in relation to sea-ice at the shelf break of the eastern Bering Sea: implications for off-shelf carbon export. J. Geophys. Res. Ocean. 118, 5504–5522. https://doi.org/10.1002/jgrc.20366.

Billett, D.S.M., Bett, B.J., Reid, W.D.K., Boorman, B., Priede, I.G., 2010. Long-term change in the abyssal NE atlantic: the 'amperima event' revisited. Deep Sea Res. Part II Top. Stud. Oceanogr. 57, 1406–1417. https://doi.org/10.1016/j.dsr2.2009.02.001.

Bol, R., Henson, S.A., Rumyantseva, A., Briggs, N., 2018. High-frequency variability of small-particle carbon export flux in the Northeast Atlantic. Global Biogeochem. Cycles 32, 1803–1814. https://doi.org/10.1029/2018GB005963.

Borrione, I., Schlitzer, R., 2013. Distribution and recurrence of phytoplankton blooms around South Georgia, Southern Ocean. Biogeosciences 10, 217–231. https://doi.org/10.5194/bg-10-217-2013.

Boscolo-Galazzo, F., Crichton, K.A., Barker, S., Pearson, P.N., 2018. Temperature dependency of metabolic rates in the upper ocean: a positive feedback to global climate change? Global Planet. Change 170, 201–212. https://doi.org/10.1016/j.gloplacha.2018.08.017.

Boyd, P.W., Newton, P.P., 1999. Does planktonic community structure determine downward particulate organic carbon flux in different oceanic provinces? Deep-Sea Res. Part I Oceanogr. Res. Pap. 46, 63–91. https://doi.org/10.1016/S0967-0637(98)00066-1.

Brandon, M.A., Murphy, E.J., Trathan, P.N., Bone, D.G., 2000. Physical oceanographic conditions to the northwest of the sub-Antarctic Island of South Georgia. J. Geophys. Res. 105 (C10), 23983–23996. https://doi.org/10.1029/2000JC900098.

Briggs, N., Dall'Olmo, G., Claustre, H., 2020. Major role of particle fragmentation in regulating biological sequestration of CO 2 by the oceans. Science 367 (80), 791–793. https://doi.org/10.1126/science.aay1790.

Briggs, N., Guðmundsson, K., Cetinić, I., D'Asaro, E., Rehm, E., Lee, C., Perry, M.J., 2018. A multi-method autonomous assessment of primary productivity and export efficiency in the springtime North Atlantic. Biogeosciences 15, 4515–4532. https://doi.org/10.5194/bg-15-4515-2018.

Briggs, N., Perry, M.J., Cetinić, I., Lee, C., D'Asaro, E., Gray, A.M., Rehm, E., 2011. High-resolution observations of aggregate flux during a sub-polar North Atlantic spring bloom. Deep-Sea Res. Part I Oceanogr. Res. Pap. 58, 1031–1039. https://doi.org/10.1016/j.dsr.2011.07.007.

Buesseler, K.O., Boyd, P.W., 2009. Shedding light on processes that control particle export and flux attenuation in the twilight zone of the open ocean. Limnol. Oceanogr. 54, 1210–1232. https://doi.org/10.4319/lo.2009.54.4.1210.

Cael, B.B., Bisson, K., 2018. Particle flux parameterizations: quantitative and mechanistic similarities and differences. Front. Mar. Sci. 5 https://doi.org/10.3389/fmars.2018.00395.

Cartapanis, O., Bianchi, D., Jaccard, S.L., Galbraith, E.D., 2016. Global pulses of organic carbon burial in deep-sea sediments during glacial maxima. Nat. Commun. 7, 10796 https://doi.org/10.1038/ncomms10796.

Cavan, E.L., Laurenceau-Cornec, E.C., Bressac, M., Boyd, P.W., 2019. Exploring the ecology of the mesopelagic biological pump. Prog. Oceanogr. 176, 102125 https://doi.org/10.1016/j.pocean.2019.102125.

Cavan, E.L., Trimmer, M., Shelley, F., Sanders, R., 2017. Remineralization of particulate organic carbon in an ocean oxygen minimum zone. Nat. Commun. 8, 14847 https://doi.org/10.1038/ncomms14847.

Ceballos-Romero, E., Le Moigne, F.A.C., Henson, S., Marsay, C.M., Sanders, R.J., García-Tenorio, R., Villa-Alfageme, M., 2016. Influence of bloom dynamics on Particle Export Efficiency in the North Atlantic: a comparative study of radioanalytical techniques and sediment traps. Mar. Chem. 186, 198–210. https://doi.org/10.1016/j.marchem.2016.10.001.

Cook, K.B., Belcher, A., Bondyale Juez, D., Stowasser, G., Fielding, S., Saunders, R.A., Elsafi, M.A., Wolff, G.A., Blackbird, S., Tarling, G.A., Mayor, D.J. (this issue) Carbon budgets of Scotia Sea mesopelagic zooplankton and micronekton 1 communities during austral spring, Deep Sea Res. II.

Cram, J.A., Weber, T., Leung, S.W., McDonnell, A.M.P., Liang, J.-H., Deutsch, C., 2018. The role of particle size, ballast, temperature, and oxygen in the sinking flux to the deep sea. Global Biogeochem. Cycles 32, 858–876. https://doi.org/10.1029/2017GB005710.

Crichton, K.A., Wilson, J.D., Ridgwell, A., Pearson, P.N., 2021. Calibration of temperature-dependent ocean microbial processes in the cGENIE.muffin (v0.9.13) Earth system model. Geosci. Model Dev. (GMD) 14, 125–149. https://doi.org/10.5194/gmd-14-125-2021.

Devol, A.H., Hartnett, H.E., 2001. Role of the oxygen-deficient zone in transfer of organic carbon to the deep ocean. Limnol. Oceanogr. 46, 1684–1690. https://doi.org/10.4319/lo.2001.46.7.1684.

DeVries, T., Weber, T., 2017. The export and fate of organic matter in the ocean: new constraints from combining satellite and oceanographic tracer observations. Global Biogeochem. Cycles 31, 535–555. https://doi.org/10.1002/2016GB005551.

Dunne, J.P., Armstrong, R.A., Gnanadesikan, A., Sarmiento, J.L., 2005. Empirical and mechanistic models for the particle export ratio. Global Biogeochem. Cycles 19. https://doi.org/10.1029/2004GB002390 n/a-n/a.

Estapa, M.L., Feen, M.L., Breves, E., 2019. Direct observations of biological carbon export from profiling floats in the subtropical North Atlantic. Global Biogeochem. Cycles 33, 282–300. https://doi.org/10.1029/2018GB006098.

Fan, G., Han, Z., Ma, W., Chen, S., Chai, F., Mazloff, M.R., Pan, J., Zhang, H., 2020. Southern Ocean carbon export efficiency in relation to temperature and primary productivity. Sci. Rep. 10, 13494 https://doi.org/10.1038/s41598-020-70417-z.

Giering, S.L.C., Sanders, R., Martin, A.P., Henson, S.A., Riley, J.S., Marsay, C.M., Johns, D.G., 2017. Particle flux in the oceans: challenging the steady state assumption. Global Biogeochem. Cycles 31, 159–171. https://doi.org/10.1002/2016GB005424.

Giering S.L.C, Sanders, R., Blackbird, S., Briggs, N., Carvalho, F., East, H., Espinola, B., Henson, S.A., Kiriakoulakis, K., Iversen, M.H., Lampitt, R.S., Pabortsava, K., Pebody, C., Peele, K., Preece, C., Saw, K., Villa-Alfageme, M., Wolff, G.A., (this issue). Vertical imbalance in organic carbon budgets is indicative of a missing vertical transfer during a phytoplankton bloom near South Georgia (COMICS1). Deep Sea Res II.

Guidi, L., Legendre, L., Reygondeau, G., Uitz, J., Stemmann, L., Henson, S.A., 2015. A new look at ocean carbon remineralization for estimating deepwater sequestration. Global Biogeochem. Cycles 29, 1044–1059. https://doi.org/10.1002/2014GB005063.

Guidi, L., Stemmann, L., Jackson, G.A., Ibanez, F., Claustre, H., Legendre, L., Picheral, M., Gorskya, G., 2009. Effects of phytoplankton community on production, size, and export of large aggregates: a world-ocean analysis. Limnol. Oceanogr. 54, 1951–1963. https://doi.org/10.4319/lo.2009.54.6.1951.

Hartman, S.E., Bett, B.J., Durden, J.M., Henson, S.A., Iversen, M., Jeffreys, R.M., Horton, T., Lampitt, R., Gates, A.R., 2021. Enduring science: three decades of observing the Northeast Atlantic from the porcupine abyssal plain sustained observatory (PAP-SO). Prog. Oceanogr. 191, 102508 https://doi.org/10.1016/j.pocean.2020.102508.

Heimbürger, L.-E., Lavigne, H., Migon, C., D'Ortenzio, F., Estournel, C., Coppola, L., Miquel, J.-C., 2013. Temporal variability of vertical export flux at the DYFAMED time-series station (Northwestern Mediterranean Sea). Prog. Oceanogr. 119, 59–67. https://doi.org/10.1016/j.pocean.2013.08.005.

Henson, S., Lampitt, R., Johns, D., 2012a. Variability in phytoplankton community structure in response to the North Atlantic Oscillation and implications for organic carbon flux. Limnol. Oceanogr. 57, 1591–1601. https://doi.org/10.4319/lo.2012.57.6.1591.

Henson, S., Le Moigne, F., Giering, S., 2019. Drivers of carbon export efficiency in the global ocean. Global Biogeochem. Cycles 33, 891–903. https://doi.org/10.1029/2018GB006158.

Henson, S.A., Sanders, R., Madsen, E., 2012b. Global patterns in efficiency of particulate organic carbon export and transfer to the deep ocean. Global Biogeochem. Cycles 26. https://doi.org/10.1029/2011GB004099 n/a-n/a.

Henson, S.A., Sanders, R., Madsen, E., Morris, P.J., Le Moigne, F., Quartly, G.D., 2011. A reduced estimate of the strength of the ocean's biological carbon pump. Geophys. Res. Lett. 38 https://doi.org/10.1029/2011GL046735 n/a-n/a.

Henson, S.A., Yool, A., Sanders, R., 2015. Variability in efficiency of particulate organic carbon export: a model study. Global Biogeochem. Cycles 29, 33–45. https://doi.org/10.1002/2014GB004965.

Honda, M.C., Imai, K., Nojiri, Y., Hoshi, F., Sugawara, T., Kusakabe, M., 2002. The biological pump in the northwestern North Pacific based on fluxes and major components of particulate matter obtained by sediment-trap experiments (1997–2000). Deep Sea Res. Part II Top. Stud. Oceanogr. 49, 5595–5625. https://doi.org/10.1016/S0967-0645(02)00201-1.

Iversen, M., 2003. Carbon export in the ocean: a biologist's perspective. Ann. Rev. Mar. Sci 15, 357–381. https://doi.org/10.1146/annurev-marine-032122-035153.

Lam, P.J., Doney, S.C., Bishop, J.K.B., 2011. The dynamic ocean biological pump: insights from a global compilation of particulate organic carbon, CaCO 3 , and opal concentration profiles from the mesopelagic. Global Biogeochem. Cycles 25. https://doi.org/10.1029/2010GB003868 n/a- n/a.

Le Moigne, F.A.C., Henson, S.A., Sanders, R.J., Madsen, E., 2013. Global database of surface ocean particulate organic carbon export fluxes diagnosed from the 234Th technique. Earth Syst. Sci. Data 5, 295–304. https://doi.org/10.5194/essd-5-295-2013.

Lima, I.D., Lam, P.J., Doney, S.C., 2014. Dynamics of particulate organic carbon flux in a global ocean model. Biogeosciences 11, 1177–1198. https://doi.org/10.5194/bg-11-1177-2014.

Lombard, F., Boss, E., Waite, A.M., Vogt, M., Uitz, J., Stemmann, L., Sosik, H.M., Schulz, J., Romagnan, J.-B., Picheral, M., Pearlman, J., Ohman, M.D., Niehoff, B., Möller, K.O., Miloslavich, P., Lara-Lpez, A., Kudela, R., Lopes, R.M., Kiko, R., Karp-Boss, L., Jaffe, J.S., Iversen, M.H., Irisson, J.-O., Fennel, K., Hauss, H., Guidi, L., Gorsky, G., Giering, S.L.C., Gaube, P., Gallager, S., Dubelaar, G., Cowen, R.K., Carlotti, F., Briseño-Avena, C., Berline, L., Benoit-Bird, K., Bax, N., Batten, S., Ayata, S.D., Artigas, L.F., Appeltans, W., 2019. Globally consistent quantitative observations of planktonic ecosystems. Front. Mar. Sci. 6 https://doi.org/10.3389/fmars.2019.00196.

Longhurst, A., 2006. Ecological Geography of the Sea, second ed. Academic Press.

Manno, C., Stowasser, G., Fielding, S., Apeland, B., Tarling, G., 2022. Deep carbon export peaks are driven by different biological pathways during the extended Scotia Sea (Southern Ocean) bloom. Deep Sea Res. II 205. https://doi.org/10.1016/j.dsr2.2022.105183.

Marinov, I., Gnanadesikan, A., Toggweiler, J.R., Sarmiento, J.L., 2006. The Southern Ocean biogeochemical divide. Nature 441, 964–967. https://doi.org/10.1038/nature04883.

Marsay, C.M., Sanders, R.J., Henson, S.A., Pabortsava, K., Achterberg, E.P., Lampitt, R.S., 2015. Attenuation of sinking particulate organic carbon flux through the mesopelagic ocean. Proc. Natl. Acad. Sci. USA 112, 1089–1094. https://doi.org/10.1073/pnas.1415311112.

Martin, J.H., Knauer, G.A., Karl, D.M., Broenkow, W.W., 1987. VERTEX: carbon cycling in the northeast Pacific. Deep-Sea Res., Part A 34, 267–285. https://doi.org/10.1016/0198-0149(87)90086-0.

Matano, R.P., Combes, V., Young, E.F., Meredith, M.P., 2020. Modeling the impact of ocean circulation on chlorophyll blooms around South Georgia, Southern Ocean. J. Geophys. Res. Oceans 125. https://doi.org/10.1029/2020JC016391 e2020JC016391.

McGill, P.R., Henthorn, R.G., Bird, L.E., Huffard, C.L., Klimov, D.V., Smith, K.L., 2016. Sedimentation event sensor: new ocean instrument for in situ imaging and fluorometry of sinking particulate matter. Limnol Oceanogr. Methods 14, 853–863. https://doi.org/10.1002/lom3.10131.

Meredith, M.P., 2003. Southern ACC Front to the northeast of SouthSouth Georgia: pathways, characteristics, and fluxes. J. Geophys. Res. 108, 3162. https://doi.org/10.1029/2001JC001227.

Mignot, A., Ferrari, R., Claustre, H., 2018. Floats with bio-optical sensors reveal what processes trigger the North Atlantic bloom. Nat. Commun. 9, 190. https://doi.org/10.1038/s41467-017-02143-6.

Mosby, H., 1934. The waters of the atlantic antarctic ocean. In: Scientific Results of the Norwegian Antarctic Expedition, 1927-1928, p. 131. Oslo.

Mouw, C.B., Barnett, A., McKinley, G.A., Gloege, L., Pilcher, D., 2016. Phytoplankton size impact on export flux in the global ocean. Global Biogeochem. Cycles 30, 1542–1562. https://doi.org/10.1002/2015GB005355.

Owens, S.A., Pike, S., Buesseler, K.O., 2015. Thorium-234 as a tracer of particle dynamics and upper ocean export in the Atlantic Ocean. Deep Sea Res. Part II Top. Stud. Oceanogr. 116, 42–59. https://doi.org/10.1016/j.dsr2.2014.11.010.

Parekh, P., Dutkiewicz, S., Follows, M.J., Ito, T., 2006. Atmospheric carbon dioxide in a less dusty world. Geophys. Res. Lett. 33, L03610 https://doi.org/10.1029/2005GL025098.

Passow, U., Carlson, C., 2012. The biological pump in a high CO2 world. Mar. Ecol. Prog. Ser. 470, 249–271. https://doi.org/10.3354/meps09985.

Rembauville, M., Salter, I., Leblond, N., Gueneugues, A., Blain, S., 2015. Export fluxes in a naturally iron-fertilized area of the Southern Ocean – Part 1: seasonal dynamics of particulate organic carbon export from a moored sediment trap. Biogeosciences 12, 3153–3170. https://doi.org/10.5194/bg-12-3153-2015.

Sanders, R.J., Henson, S.A., Martin, A.P., Anderson, T.R., Bernardello, R., Enderlein, P., Fielding, S., Giering, S.L.C., Hartmann, M., Iversen, M., Khatiwala, S., Lam, P., Lampitt, R., Mayor, D.J., Moore, M.C., Murphy, E., Painter, S.C., Poulton, A.J., Saw, K., Stowasser, G., Tarling, G.A., Torres-Valdes, S., Trimmer, M., Wolff, G.A., Yool, A., Zubkov, M., 2016. Controls over Ocean Mesopelagic interior carbon storage (COMICS): fieldwork, synthesis, and modeling efforts. Front. Mar. Sci. 3 https://doi.org/10.3389/fmars.2016.00136.

Siegel, D., Deuser, W.G., 1997. Trajectories of sinking particles in the Sargasso Sea: modeling of statistical funnels above deep-ocean sediment traps. Deep-Sea Res. Part I Oceanogr. Res. Pap. 44 (9–10), 1519–1541. https://doi.org/10.1016/S0967-0637(97)00028-9.

Smetacek, V., von Brockel, K., Zeitzschel, B., Zenk, W., 1978. Sedimentation of particulate matter during a phytoplankton spring bloom in relation to the hydrographical regime. Mar. Biol. 47, 211–226.

Smith, K.L., Ruhl, H.A., Huffard, C.L., Messié, M., Kahru, M., 2018. Episodic organic carbon fluxes from surface ocean to abyssal depths during long-term monitoring in NE Pacific. Proc. Natl. Acad. Sci. USA 115, 12235–12240. https://doi.org/10.1073/pnas.1814559115.

Smith, K.L., Ruhl, H.A., Kahru, M., Huffard, C.L., Sherman, A.D., 2013. Deep ocean communities impacted by changing climate over 24 y in the abyssal northeast Pacific Ocean. Proc. Natl. Acad. Sci. USA 110, 19838–19841. https://doi.org/10.1073/pnas.1315447110.

Stock, C.A., Dunne, J.P., Fan, S., Ginoux, P., John, J., Krasting, J.P., Laufkötter, C., Paulot, F., Zadeh, N., 2020. Ocean biogeochemistry in GFDL's earth system model 4.1 and its response to increasing atmospheric CO 2. J. Adv. Model. Earth Syst. 12 https://doi.org/10.1029/2019MS002043.

Uchida, T., Balwada, D., Abernathey, R., Prend, C.J., Boss, E., Gille, S.T., 2019. Southern Ocean phytoplankton blooms observed by biogeochemical floats. J. Geophys. Res. Ocean. 124, 7328–7343. https://doi.org/10.1029/2019JC015355.

Venables, H., Meredith, M.P., Atkinson, A., Ward, P., 2012. Fronts and habitat zones in the Scotia Sea. Deep Sea Res. Part II Top. Stud. Oceanogr. 59–60, 14–24. https://doi.org/10.1016/j.dsr2.2011.08.012.

Verdy, A., Dutkiewicz, S., Follows, M.J., Marshall, J., Czaja, A., 2007. Carbon dioxide and oxygen fluxes in the Southern Ocean: mechanisms of interannual variability. Global Biogeochem. Cycles 21. https://doi.org/10.1029/2006GB002916 n/a-n/a.

Villa-Alfageme, M., Briggs, N., Ceballos-Romero, E., de Soto, F.C., Manno, C., Giering, S. L.C., (this issue). Seasonal variations of sinking velocities in Austral diatom blooms: lessons learned from COMICS I. Deep Sea Res. II.

Weber, T., Cram, J.A., Leung, S.W., DeVries, T., Deutsch, C., 2016. Deep ocean nutrients imply large latitudinal variation in particle transfer efficiency. Proc. Natl. Acad. Sci. USA 113, 8606–8611. https://doi.org/10.1073/pnas.1604414113.

Wiedmann, I., Ceballos-Romero, E., Villa-Alfageme, M., Renner, A.H.H., Dybwad, C., Jagt, H., Svensen, C., Assmy, P., Wiktor, J.M., Tatarek, A., Różańska-Pluta, M., Iversen, M.H., 2020. Arctic observations identify phytoplankton community

composition as driver of carbon flux attenuation. Geophys. Res. Lett. 47 https://doi.org/10.1029/2020GL087465.